Original article

MOLECULAR METABOLISM

E4orf1 induction in adipose tissue promotes insulin-independent signaling in the adipocyte

Christine M. Kusminski [1], Violeta I. Gallardo-Montejano [2], Zhao V. Wang [1], Vijay Hegde [3,5], Perry E. Bickel [2], Nikhil V. Dhurandhar [3,5,], Philipp E. Scherer [1,4,*]**

ABSTRACT

Background/Purpose: Type 2 diabetes remains a worldwide epidemic with major pathophysiological changes as a result of chronic insulin resistance. Insulin regulates numerous biochemical pathways related to carbohydrate and lipid metabolism.
Methods: We have generated a novel mouse model that allows us to constitutively activate, in an inducible fashion, the distal branch of the insulin signaling transduction pathway specifically in adipocytes.
Results: Using the adenoviral 36 E4orf1 protein, we chronically stimulate locally the Ras-ERK-MAPK signaling pathway. At the whole body level, this leads to reduced body-weight gain under a high fat diet challenge. Despite overlapping glucose tolerance curves, there is a reduced requirement for insulin action under these conditions. The mice further exhibit reduced circulating adiponectin levels that ultimately lead to impaired lipid clearance, and inflamed and fibrotic white adipose tissues. Nevertheless, they are protected from diet-induced hepatic steatosis. As we observe constitutively elevated p-Akt levels in the adipocytes, even under conditions of low insulin levels, this pinpoints enhanced Ras-ERK-MAPK signaling in transgenic adipocytes as a potential alternative route to bypass proximal insulin signaling events.
Conclusion: We conclude that E4orf1 expression in the adipocyte leads to enhanced baseline activation of the distal insulin signaling node, yet impaired insulin receptor stimulation in the presence of insulin, with important implications for the regulation of adiponectin secretion. The resulting systemic phenotype is complex, yet highlights the powerful nature of manipulating selective branches of the insulin signaling network within the adipocyte.

Keywords Adipose tissue; Adipocyte; Diabetes; Insulin signaling; Obesity; Adenovirus

1. INTRODUCTION

Insulin signaling regulates whole-body glucose and lipid homeostasis primarily through actions on peripheral tissues, such as the liver, skeletal muscle and white adipose tissue (WAT) as well as in the brain. Upon stimulation by insulin, signals are transduced from the insulin receptor to propagate two main downstream branches, the PI3K-Akt pathway and the Ras-MAPK pathway. These orchestrate a plethora of biological functions on growth and metabolism, such as proliferation, differentiation, survival, glucose uptake and lipolysis, respectively. Under conditions of chronic nutrient excess, such as diet-induced obesity-associated type 2 diabetes mellitus (T2DM), insulin signaling is impaired. As such, peripheral tissues develop a resistance to insulin, a central feature that culminates in T2DM [1]. Understanding the intricate perturbations in the insulin signaling pathway during obesity is therefore paramount for the development of novel therapeutics to treat T2DM and its' related complications.

Over the decades, extensive efforts have focused on the various nodes of regulation within the insulin signaling pathway and the points of crosstalk that exist with other transduction cascades during insulin resistance [2]. WAT and the adipocyte itself are major regulators of whole body insulin sensitivity and energy homeostasis, with targeted defects in insulin action in adipocytes resulting in systemic insulin resistance [3–5]. Studies have attributed defective Akt signaling in adipocytes critical for the development of insulin resistance, as adipose-specific Akt2 knockout mice exhibit impaired insulin-stimulated glucose-uptake [6]. Bluher and colleagues generated mice with a fat-specific disruption in the insulin receptor gene (FIRKO mice) that display defective insulin-stimulated glucose uptake. These mice are however protected from obesity and glucose intolerance [7]. Ussar et al. described the cell-surface proteoglycan glypican-4 interacting directly

[1]Touchstone Diabetes Center, Department of Internal Medicine, The University of Texas Southwestern Medical Center, Dallas, TX, USA [2]Division of Endocrinology, Department of Internal Medicine, The University of Texas Southwestern Medical Center, Dallas, TX, USA [3]Department of Infection and Obesity Laboratory, Pennington Biomedical Research Center, Baton Rouge, LA, USA [4]Department of Cell Biology, The University of Texas Southwestern Medical Center, Dallas, TX, USA

[5] Current address: Department of Nutritional Sciences, Texas Tech University, Lubbock, TX, USA.

*Corresponding author. Touchstone Diabetes Center, Department of Internal Medicine, The University of Texas Southwestern Medical Center, Dallas, TX, USA. Tel.: +1 (214) 648 8715; fax: +1 (214) 648 8720. E-mail: philipp.scherer@utsouthwestern.edu (P.E. Scherer).

**Corresponding author. Current address: Department of Nutritional Sciences, Texas Tech University, Lubbock, TX, USA. Tel.: +1 (806) 834 6446. E-mail: Nikhil.Dhurandhar@TTU.EDU (N.V. Dhurandhar).

Received June 23, 2015 • Revision received July 8, 2015 • Accepted July 13, 2015 • Available online 26 July 2015

http://dx.doi.org/10.1016/j.molmet.2015.07.004

with the insulin receptor to enhance insulin sensitivity, albeit only in the absence of insulin [8]. There has been controversy as to which defect in the insulin signaling pathway is the major contributor to insulin resistance, with a discordance evident between upstream proximal components (the insulin receptor or insulin receptor substrate-1 [IRS-1]) [9–12] *versus* downstream distal signaling (AS160) [13], or at the level of Akt [14]. The specific step of the insulin signaling pathway at which a deficiency in insulin signaling is induced can thus contribute to major differences in phenotypic outcomes. This holds true even for differential interference along the pathway within a single tissue.

An example of alternate phenotypic outcomes following perturbation at different branches of the insulin signaling pathway is the insulin-mediated regulation of adiponectin release into the system. As a circulating adipokine, adiponectin enhances insulin sensitivity in models of insulin resistance [15,16]. However, insulin signaling within the adipocyte exerts differential effects on adiponectin release from adipocytes. Patients with genetically defective insulin receptors, by definition components of the proximal insulin signaling branch, harbor severe insulin resistance, yet paradoxically exhibit hyperadiponectinemia [17,18]. Conversely, genetic mutations in Akt-2, a distal factor in the insulin signaling node, result in low adiponectin levels. The generalized insulin resistance observed in obese patients with T2DM, also results in lower adiponectin levels. It is therefore evident that manipulating different segments of the insulin transduction cascade, whether proximal or distal, exerts profoundly differential effects on adiponectin production and whole-body insulin sensitivity. This further highlights the complexity of the relationship of adiponectin with the various components of the insulin signal transduction modules in the adipocyte. Identifying new targets impacting the insulin signal transduction cascade has the potential to decipher how perturbing the different nodes of the insulin signaling pathway within adipocytes alters whole-body insulin sensitivity.

The adenoviral gene product E4orf1 encodes a 14-kDa polypeptide that enhances glucose metabolism in a PI3K-independent manner [19]. Recent *in vitro* studies have demonstrated E4orf1 to exert insulin-independent or 'insulin-sparing' actions that bypass insulin receptor signaling to promote cellular glucose uptake in adipocytes. Studies utilizing 3T3-L1 adipocytes revealed that E4orf1 directly inhibits IRS1/2 phosphorylation in the insulin signaling pathway [20,21]. Synergistically, and unaffected by an insulin receptor knockdown, E4orf1 enhances Ras activity to activate PI3K and subsequent phosphorylation of the PI3K downstream target PKB/Akt to promote membrane translocation of Glut4, in the absence of insulin [20–23]. However, the functional role that E4orf1 exerts on insulin signaling in adipocytes *in vivo,* particularly in the context of obesity and T2DM, is yet to be established. We therefore set out to test how inducing E4orf1 in adipocytes in an *in vivo* setting could serve as a novel means to study the different branches of the insulin signaling pathway and further, to provide a model for investigating the role of insulin in the regulation of adiponectin secretion from adipocytes. We wanted to explore how the E4orf1-mediated 'insulin-sparing' effects have an impact on systemic metabolic parameters *in vivo.* To avoid any developmental issues, we generated and characterized an inducible mouse model of E4orf1 expression in adipocytes in which we express the protein exclusively in the mature adipocyte.

2. MATERIALS AND METHODS

2.1. Animals

All animal experimental protocols were approved by the Institutional Animal Care and Use Committee of University of Texas Southwestern Medical Center at Dallas. To generate a doxycycline (Dox)-inducible mouse model of E4orf1 overexpression, E4orf1 cDNA was amplified and engineered into pENTR vector (Invitrogen) and verified by sequencing from both ends (Genewiz). To facilitate cloning, we engineered Gateway components (Invitrogen) into pTRE vector (Clontech). A rabbit β-globin 3′UTR was included to stabilize the transcript and enhance the translation. This pTRE-Gateway-3′UTR vector was used for one-step cloning of E4orf1 into pTRE construct by recombination. The expression of E4orf1 is controlled by 7 tandem repeats of tetracycline responsive elements in front of a minimum CMV promoter. The pTRE-E4orf1 DNA was linearized by *Xmn* I, *Ale* I, *Cla* I and *Ahd* I digestion. A 5.2-kb fragment was purified by Elutip-D and injected into embryos of pure C57/Bl6 background by the transgenic core facility at UTSW. Transgene-positive TRE-E4orf1 offspring were genotyped using PCR with the primer set: 5′-GGCA-TACTAACCCAGTCCGATG and 5′-AATCACTCTCTCCAGCAGCAGG. Adiponectin-rtTA mice were generated as previously described [24]. All overexpression experiments were performed in a pure C57/Bl6 background. All experiments were conducted using littermate-controlled male WT mice and male E4orf1 transgenic mice. Mice were fed a standard chow diet (number 5058, LabDiet, St. Louis, MO), a Dox-chow diet (600 mg/kg Dox; BioServ, Frenchtown, NJ) or a Dox-HFD (600 mg/kg Dox; BioServ). All experiments were initiated at approximately 6–12-weeks of age.

2.2. Systemic tests

For the OGTT, mice were fasted for 3 h prior to administration of glucose (2.5 g/kg body-weight by gastric gavage). At the indicated time-points, venous blood samples were collected in heparin-coated capillary tubes from the tail-vein. Glucose levels were measured using an oxidase-peroxidase assay (Sigma–Aldrich). Mice did not have access to food throughout the experiment. For TG clearance, mice were fasted (~14–16 h), then gavaged 20% Intra-lipid (15 ul/g body-weight; Fresenius Kabi Clyton, L.P., Clayton, NC). Blood was collected at timed intervals then assayed for TG levels (Infinity; Thermo Fisher Scientific) and FFA levels (NEFA-HR(2); Wako Pure Chemical Industries, Tokyo, Japan). Insulin and adiponectin levels were measured using commercial ELISA kits (Millipore Linco Research, St. Charles, MO). Glycerol and glucose levels were determined using a free glycerol reagent and an oxidase-peroxidase assay, respectively (Sigma–Aldrich).

2.3. Quantitative real-time PCR, RNA deep sequencing and Illumina microarray

Subcutaneous white adipose tissues were excised from mice and immediately snap-frozen in liquid nitrogen. Total RNA was isolated following tissue homogenization in Trizol (Invitrogen, Carslbad, CA) utilizing a TissueLyser (MagNA Lyser, Roche), then isolated using an RNeasy RNA extraction kit (Qiagen). The quality and quantity of the RNA was determined by absorbance at 260/280 nm cDNA was prepared by reverse transcribing 1 ug of RNA with an iScript cDNA Synthesis Kit (BioRad, Hercules CA). Results were calculated using the threshold cycle method [25], with β-actin utilized for normalization. For RNA deep sequencing, total sWAT RNA (10 ng) was submitted for transcriptome sequencing (RNA-Seq). For Illumina microarray, total cDNA was synthesized from BAT and spotted onto a mouse Illumina BeadArray platform (Illumina, Inc.). Fold-changes and significance were calculated based on three independent replicates. Key gene lists and cluster analyses of the data sets were performed using Ingenuity software (Ingenuity Systems Inc.).

2.4. Immunoblotting

For analysis of cytoplasmic fractions, frozen tissues were homogenized using a TissueLyser (MagNA Lyser, Roche) in TNET buffer (50 mM Tris—HCl [pH 7.6], 150 mM NaCl, 5 mM EDTA, phosphatase inhibitors [Sigma Aldrich] and protease inhibitors [Roche]), followed by low centrifugation and removal of any adipose-layer present. For nuclear extractions, frozen tissues were homogenized in RIPA buffer (25 mM Tris—HCl [pH 7.6], 150 mM NaCl, 1% sodium deoxycholate and 0.1% SDS). For nuclear isolations, a Nuclear Extraction Kit was utilized (Active Motif, Carlsbad, CA). Following addition of Triton X-100 to a final concentration of 1%, protein concentrations were determined using a bicinchoninic acid assay (BCA) kit (Pierce). Proteins were resolved on either a 4—12% bis-Tris get (Invitrogen) or a 10—20% Tricine gel (Invitrogen) then transferred to a polyvinylidene difluoride membrane (Millipore) or a nitrocellulose membrane (Protran, Whatman GmbH, Germany), respectively. An anti-rabbit polyclonal antibody for E4orf1 was utilized (1:1,000, as previously described [20]). Phospho-Akt (Ser473) and total-Akt (Cell Signaling Technology, Inc., Boston, MA) were used (1:1,000) for insulin signaling studies. Phospho-tyrosine (Tyr) (insulin receptor [IR] and insulin receptor substrate [IRS]) (1:1,000, Cell Signaling Technology, Inc., Boston, MA), in addition to phospho-ERK and total-ERK (1:1,000, Cell Signaling Technology, Inc., Boston, MA) were also utilized for insulin signaling studies. Control primary antibodies utilized were β-actin and histone-H3 (1:1,000, Cell Signaling Technology, Inc., Boston, MA). Primary antibodies were detected using secondary IgGs labeled with infrared dyes emitting at 700 and 800 nm (1:5,000; Li-Cor Bioscience, Lincoln, NB) then visualized on a Li-Cor Odyssey infrared scanner (Li-Cor Bioscience). The scanned data were analyzed using Odyssey Version 2.1 software (Li-Cor Bioscience).

2.5. Histology and immunohistochemical (IHC) staining

The relevant fat-pads or liver tissues were excised and fixed in 10% PBS-buffered formalin for 24 h. Following paraffin embedding and sectioning (5 μm), tissues were stained with H&E or a Masson's Trichrome stain. For IHC, paraffin-embedded sections were stained using monoclonal anti-Mac2 antibodies (1:250; CEDARLANE Laboratories USA Inc., Burlington, NC).

2.6. Hepatic triglyceride content

Frozen liver tissues were utilized for lipid extraction and measurement by the UT Southwestern Medical Center Metabolic Core Facility. Briefly, ~100—150 mg frozen liver chunks were homogenized. Lipids were then extracted using the Folch procedure [26] and the chloroform phase was adjusted to equal volume, and triplicates of the samples in combination with standards, were dried down by the addition of 10 ml of 2:1 chloroform-Triton X-100 mix.

2.7. Isolation and differentiation of primary adipose stromal vascular fraction (SVF) cells

The isolation of SVF and cellular differentiation protocol was adapted from previous procedures [27]. In brief, BAT depots were dissected from 8 to 12-week old mice, washed, minced and then digested for two hours at 37 °C in digestion buffer (100 mM HEPES [pH 7.4], 120 mM NaCl, 50 mM KCl, 5 mM glucose, 1 mM $CaCl_2$, 1.5% BSA and 1 mg/ml collagenase D [Roche]). Digested BAT was then filtered through a cell strainer (100 μm) and the flow-through then centrifuged for 5 min at 600 × g. The pelleted SVF cells were re-suspended in SVF culture media (DMEM/F12, Invitrogen) supplemented with Glutamax, Pen/Strep, Gentamicin and 10% FBS, then filtered through a cell strainer (40 μm). Following centrifugation (5 min at 600 × g) cells were re-suspended in SVF culture media and seeded onto collagen-coated 6-cm tissue culture plates. Upon confluence, cells were treated with SVF medium containing dexamethasone (1 mM), insulin (5 μg/ml), isobutylmethylxanthine (0.5 mM) and rosiglitazone (RSG) (1 mM) to induce adipocyte differentiation. Then forty-eight hours post induction cells were maintained in SVF medium supplemented with insulin (5 μg/ml) and RSG (1 mM). Following seven days of differentiation, adipocytes were treated for two days with Dox-containing media (10 μg/ml) prior to harvest.

2.8. Statistics

All results are provided as means ± standard errors of the mean. All statistical analysis was performed using GraphPad Prism (San Diego, CA). Differences between the two groups over time (as indicated in the relevant figure legends) were determined by a two-way analysis of variance (ANOVA) for repeated measures. For comparison between two independent groups, a Student's *t*-test was utilized. Significance was accepted at a P value of <0.05.

3. RESULTS

3.1. Inducible, titratable and highly specific overexpression of E4orf1 in adipose tissue

To induce E4orf1 specifically in adipose tissue (AT), we generated a mouse in which the expression of E4orf1 is driven by a tetracycline-inducible promoter element (a *tet*-responsive element, or TRE). We refer to this mouse as the TRE-E4orf1 mouse. For this promoter element to be operational, the presence of the 'Tet-on' transcription factor rtTA is required. We provide this factor in an adipocyte-specific manner through a mouse that harbors the rtTA component under the control of the adiponectin promoter [24]. Upon crossing TRE-E4orf1 mice with adiponectin-rtTA mice, followed by administration of doxycycline (Dox) to the resulting pups (the "E4orf1-Tg mice"), we achieve induction of E4orf1 expression specifically within adipose tissues. Our *in vivo* system of E4orf1 overexpression is inducible, highly specific and titratable; with the latter achieved through alterations in Dox concentrations. Initial observations revealed that following one-week of Dox-chow (600 mg/kg Dox) feeding, we efficiently induce E4orf1 protein in transgenic subcutaneous white adipose tissue (sWAT), gonadal WAT (gWAT), mesenteric WAT (mWAT) and brown adipose tissue (BAT); with the highest degree of E4orf1 induction evident in BAT (Figure 1A). No induction of E4orf1 protein is observed in the liver, therefore highlighting the specificity of E4orf1 protein overexpression exclusively to adipose tissues.

Following confirmation of E4orf1 protein induction, we addressed whether overexpression of the human adenovirus 36 (Ad36E4orf1) in murine AT alters food-intake. Figure 1B highlights that no significant differences in food-intake are evident between control wild-type (WT) mice and E4orf1-Tg mice following two weeks of Dox-chow (600 mg/kg) feeding. Subsequent analyses assessing systemic parameters under baseline, metabolically *unchallenged* conditions revealed that E4orf1-Tg mice exhibit significantly higher levels of triglycerides (TAGs), free fatty acids (FFAs) and glycerol, both in the fed-state and under fasted (24 h) conditions (Figure 1C). This suggests that some degree of enhanced basal and fasting-induced lipolysis is present in E4orf1-Tg mice. Interestingly, despite *in vitro* studies documenting that E4orf1 overexpression enhances adiponectin secretion from human differentiated adipocytes [28], here we observed a marked reduction in

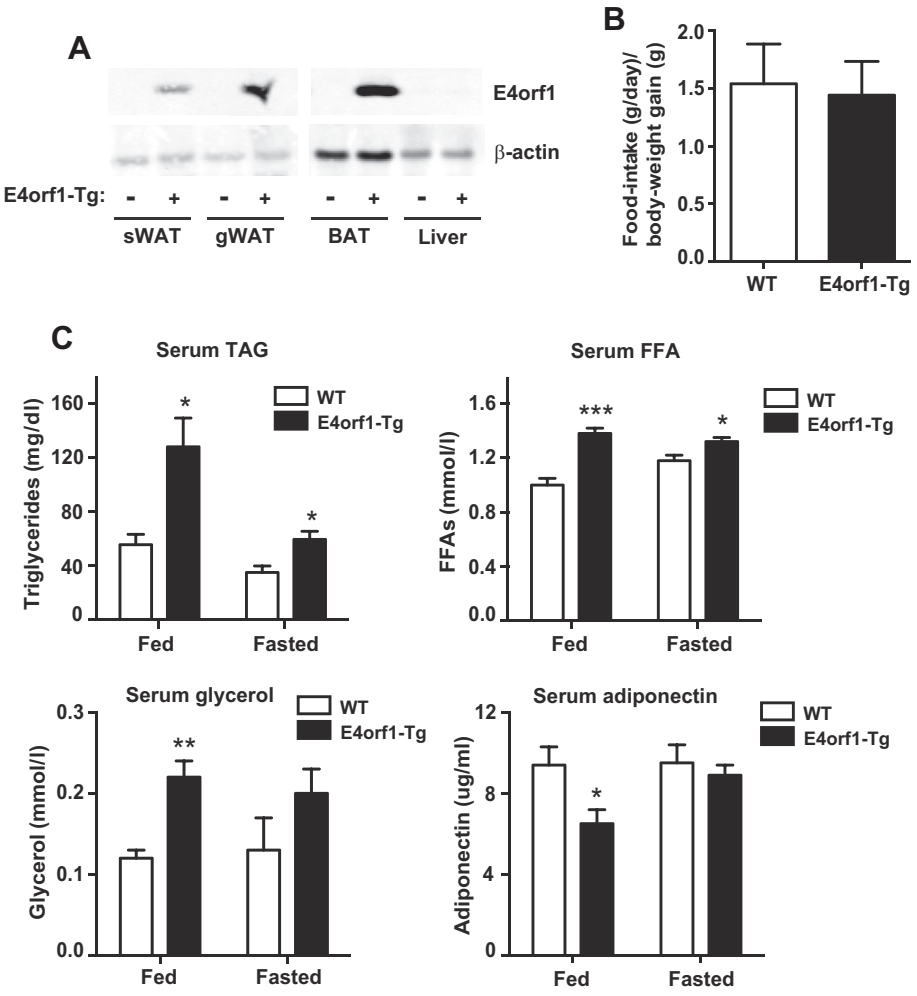

Figure 1: Adipose-tissue-specific induction of E4orf1 promotes fasting-induced lipolysis and lowering of adiponectin levels. (A) Representative Western blots showing E4orf1 protein expression levels (top panel) and β-actin (bottom panel) in subcutaneous white adipose tissue (sWAT), gonadal WAT (gWAT) and brown adipose tissue (BAT) derived from wild-type (WT) mice *versus* adipose tissue-specific E4orf1 transgenic (E4orf1-Tg) mice fed doxycycline (Dox)-chow (600 mg/kg Dox) for one-week. (B) Food-intake (g/day/body-weight gain [g]) of WT mice *versus* E4orf1-Tg mice following two-weeks of Dox-chow (600 mg/kg) feeding, ($n = 5$ per group). (C) *Ad libitum* and 24 h fasted circulating triglycerides (TAG), free fatty acid (FFA), glycerol and adiponectin levels in male C57/Bl6 WT mice *versus* E4orf1-Tg mice post two-weeks Dox-chow (600 mg/kg) feeding, ($n = 5$ per group). (Student's *t*-test, $^{*}P < 0.05$; $^{**}P < 0.01$; $^{***}P < 0.001$).

systemic adiponectin levels in E4orf1-Tg mice under *ad libitum* feeding (Figure 1C), reflecting a differential response between *in vitro* cultured and *in vivo* systems.

3.2. AT-specific E4orf1-Tg mice exhibit reduced body-weight gain during a metabolic challenge, potential *insulin-sparing* characteristics, inflamed and fibrotic WAT with minimal hepatic steatosis

To apply a metabolic challenge, we fed E4orf1-Tg mice Dox high-fat diet (Dox-HFD) (600 mg/kg) and monitored body-weights. Figure 2A shows that E4orf1-Tg mice exhibit significantly lower body-weight gain during Dox-HFD feeding. Following six weeks Dox-HFD feeding, we performed an oral glucose tolerance test (OGTT) and observed no marked differences in glucose tolerance between WT mice and E4orf1-Tg mice (Figure 2B), although baseline acute fasting (3 h) glucose levels were significantly lower in E4orf1-Tg mice compared to WT littermates (Figure 2B), suggesting possible protection from HFD-induced fasting hyperglycemia. Interestingly, E4orf1-Tg mice exhibit a profoundly lower transient insulin spike in response to the glucose load during the OGTT, in comparison to WT mice. Insulin levels were significantly lower both at baseline and throughout the duration of the OGTT (Figure 2B). We ruled out any pancreatic β-cell defects in E4orf1-Tg mice, given their normal capacity to clear a glucose bolus from circulation. *In vitro* studies have documented that E4orf1 enhances cellular glucose uptake in the *absence of insulin*, either by bypassing the insulin receptor or by sustaining activation of downstream insulin signaling components in the face of an insulin receptor knockdown [20–22], suggesting potential unique 'insulin sparing' actions of E4orf1-mediated signaling. Here, given that E4orf1-Tg mice clear exogenous glucose efficiently while not harboring any β-cell defects, yet exhibit severely lower insulin levels in doing so, our data suggest that E4orf1-Tg mice may have a lower requirement for insulin. They effectively preserve whole-body glucose clearance capacity and the distal branch of the insulin signaling cascade, with a lower requirement for insulin. We further assessed lipid clearance efficacy and observed that E4orf1-Tg mice exhibit impaired triglyceride (TG) clearance, evidenced by significantly higher systemic TG levels following an oral lipid gavage (Figure 2C). This suggests that E4orf1-Tg mice harbor an

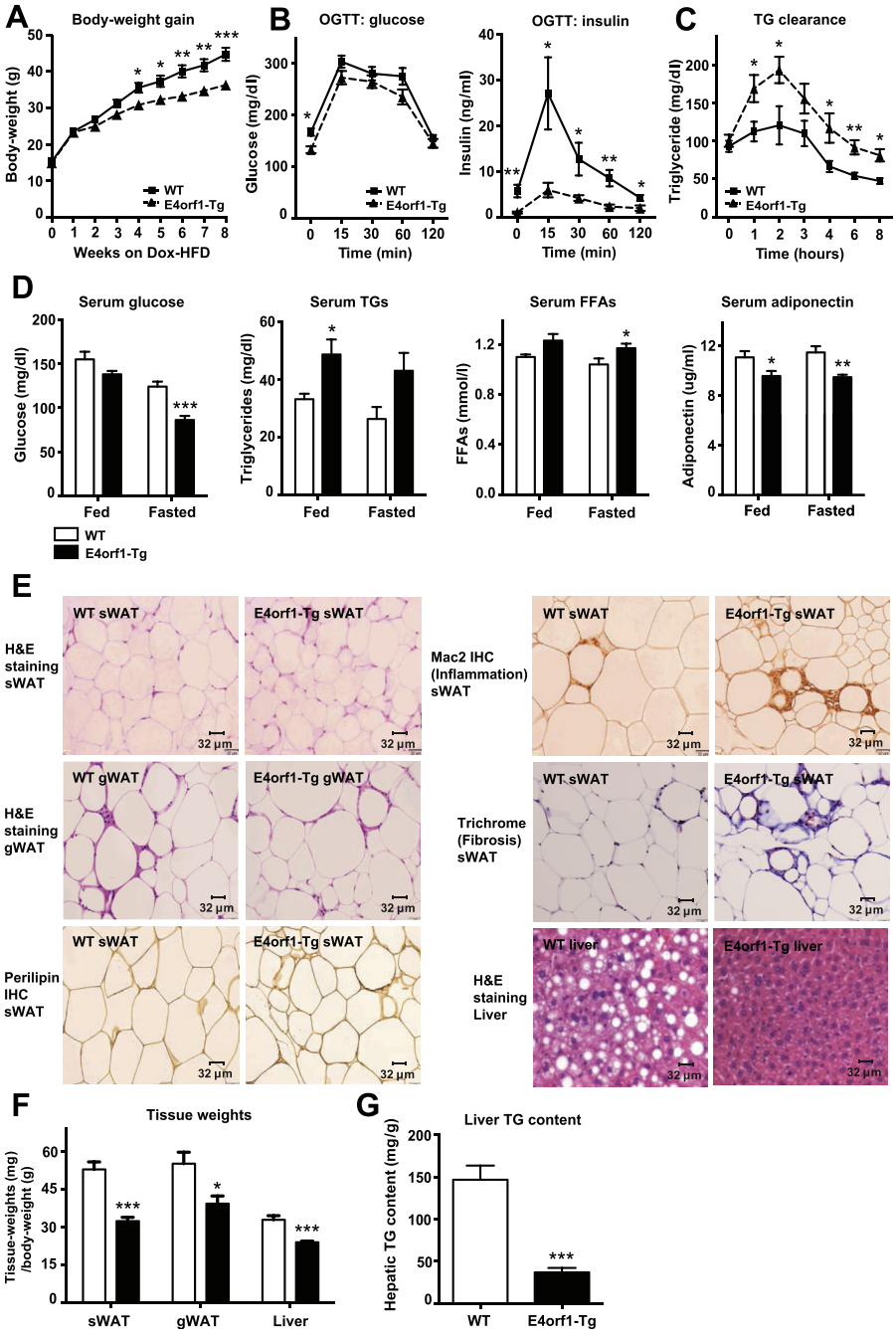

Figure 2: E4orf1-Tg mice exhibit lower body-weight gain, systemic *insulin-sparing* effects, inflamed and fibrotic WAT with minimal hepatic steatosis. (A) Body-weight gain (g) of male C57/Bl6 WT mice *versus* E4orf1-Tg mice during Dox-HFD (600 mg/kg) feeding, ($n = 7$ per group). (B) Glucose levels (left) and insulin levels (right) during an oral glucose tolerance test (OGTT) (2.5 g/kg body-weight glucose; single gavage) on male WT mice *versus* E4orf1-Tg mice, ($n = 7$ per group). (C) Triglyceride clearance test on WT mice *versus* E4orf1-Tg mice post eight-weeks Dox-HFD feeding. Mice were gavaged (20 ul/g body-weight 20% Intra-lipid) following an overnight (14–16 h fast), ($n = 7$ per group). (D) *Ad libitum* and 24 h fasted systemic glucose, TG and adiponectin levels in WT mice *versus* E4orf1-Tg mice post eight-weeks Dox-HFD (600 mg/kg) feeding, ($n = 7$ per group). (E) Representative images of H&E staining of sWAT (top left) and gWAT (middle left) tissues from WT *versus* E4orf1-Tg mice post eight-weeks Dox-HFD feeding. Representative images of perilipin immunohistochemical (IHC) staining of sWAT (bottom left) derived from WT *versus* E4orf1-Tg mice. Mac2 IHC staining (top right) and Trichrome staining (middle right) of sWAT, in addition to H&E staining of liver tissues (bottom right) from WT mice *versus* E4orf1-Tg mice post eight-weeks Dox-HFD feeding. Scale bar: 32 µm. (F) Fat-pad (sWAT and gWAT) and liver tissue weights (mg) normalized to body-weight (g), in WT mice *versus* E4orf1-Tg mice post eight-weeks Dox-HFD feeding, ($n = 7$ per group). (G) Hepatic TG content (mg/g) in livers derived from WT mice *versus* E4orf1-Tg mice post eight-weeks Dox-HFD feeding, ($n = 7$ per group). (Student's *t*-test, $^{*}P < 0.05$; $^{**}P < 0.01$; $^{***}P < 0.001$).

unfavorable systemic lipid profile. We subsequently measured various systemic parameters under *ad libitum* and fasted (24 h) conditions. While E4orf1-Tg mice weigh markedly less than their WT counterparts, no differences in the fasting-induced body-weight changes were apparent following a 24 h fast (*data not shown*). Secondly, E4orf1-Tg mice exhibit significantly lower fasting blood glucose levels (Figure 2D). Such fasting-induced hypoglycemia is consistent with *in vitro* studies demonstrating that E4orf1 confers anti-hyperglycemic

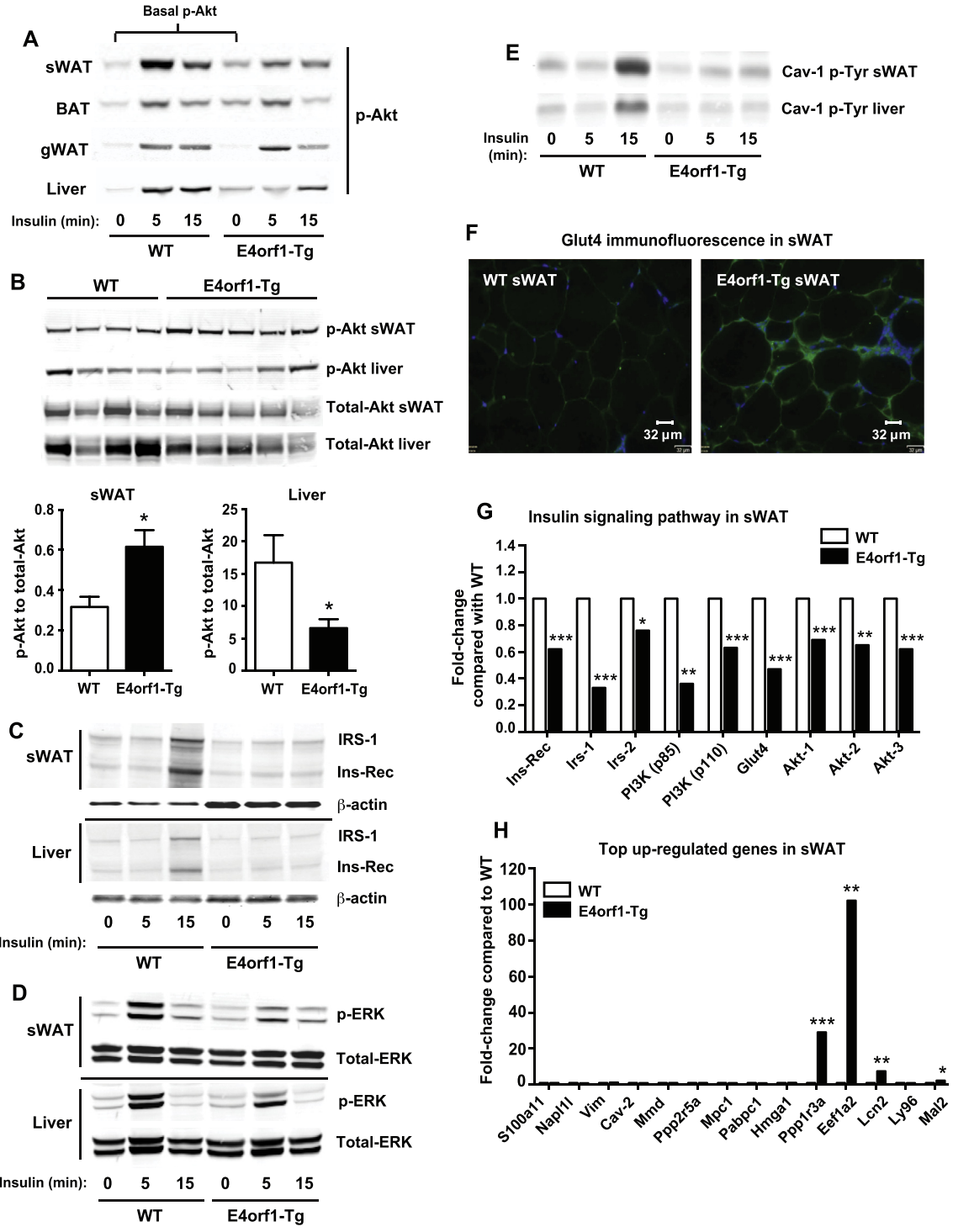

Figure 3: E4orf1 induction in adipose tissue alters components of the insulin-signaling cascade in sWAT and liver tissues. (A) Representative Western blots of phospho (p)-Akt expression (~60 kDa) in sWAT, BAT, gWAT and liver tissues from WT *versus* E4orf1-Tg mice prior to and post insulin injection (0, 5 and 15 min time-points) that were fed Dox-chow (600 mg/kg) for two-weeks. Mice were fasted overnight (~14–16 h) prior to insulin injection (1 U/kg body-weight insulin i.p). (B) Western blots of p-Akt (upper panels) and total-Akt (~60 kDa) (lower panels) in sWAT and liver tissues derived from WT mice *versus* E4orf1-Tg mice post Dox-chow (600 mg/kg) feeding. Bar graphs show p-Akt levels normalized to total-Akt levels in sWAT (left) and liver (right). (C) Western blots of the phospho-tyrosine (p-Tyr) insulin receptor β-subunit (Ins-Rec) (~97 kDa) and p-Tyr insulin receptor substrate-1 (IRS-1) (~170 kDa) in sWAT (upper panels) and liver (lower panels) tissues derived from Dox-chow (600 mg/kg) fed WT mice *versus* E4orf1-Tg mice prior and post insulin injection (5 and 15 min). The loading control β-actin is also provided. (D) Western blots of p-ERK (p-44/42 MAPK [ERK 1/2]) (Thr-202/Tyr-204) (~42/44 kDa) and total-ERK expression levels in sWAT (upper panels) and liver (lower panels) tissues derived from Dox-chow (600 mg/kg) fed WT mice *versus* E4orf1-Tg mice prior and post insulin injection (5 and 15 min). (E) Western blots of p-Caveolin (Cav)-1 (p-Tyr^{14}) (~22 kDa) in sWAT (upper panel) and liver (lower panel) tissues derived from Dox-chow (600 mg/kg) fed WT mice *versus* E4orf1-Tg mice prior and post insulin injection (5 and 15 min). (F) Representative images of Glut4 immunofluorescence staining of sWAT from WT *versus* E4orf1-Tg mice post eight-weeks Dox-HFD feeding. Scale bar: 32 µm. (G) Real-time qPCR data showing the fold-changes (in comparison to WT) in gene expression levels of key components of the insulin signaling pathway (*Ins-Rec*, *Irs-1/2*, *PI3K* [*p85/p110*], *Glut4* and *Akt-1/2/3*) in sWAT derived from WT mice *versus* E4orf1-Tg mice that underwent three-weeks of Dox-HFD (600 mg/kg) feeding. Mice were fasted for 3–4 h prior to tissue harvest ($n = 9$/group). (H) Real-time qPCR confirmation of the top significantly up-regulated genes (identified by RNA-Seq analyses) in E4orf1-Tg sWAT, when compared with WT sWAT, ($n = 9$ per group). (I) Real-time qPCR of the most significantly down-regulated genes (identified by RNA-Seq analyses) in E4orf1-Tg sWAT, when compared with WT sWAT, (n = 9 per group). (Student's *t*-test, $^{*}P < 0.05$; $^{**}P < 0.01$; $^{***}P < 0.001$).

actions by improving cellular glucose disposal [20,23]. Here, such actions of E4orf1 appear to be more effective under fasted conditions. In line with the impaired TG clearance capacity, we observed markedly higher circulating TG levels and FFA levels in E4orf1-Tg mice, when compared with WT mice (Figure 2D), implicating some degree of fasting-induced lipolysis present in metabolically challenged E4orf1-Tg mice. Similar to Dox-chow fed conditions, both in the Dox-HFD-fed-state and during fasting, E4orf1-Tg mice exhibit lower systemic adiponectin levels in comparison to their WT littermates (Figure 2D). Given that it has been established that circulating adiponectin levels are lower in states of obesity and T2DM [29–31], the reduction in adiponectin in E4orf1-Tg mice that exhibit a leaner phenotype in comparison to their WT counterparts suggests impaired production of adiponectin from WAT and further implicates that E4orf1 induction may promote WAT dysfunction and metabolically 'unhealthy' WAT expansion.

In light of the fact that we do not see measurable differences in food-intake, yet there is a significant difference in body-weight gain, we wanted to examine whether the differences were large enough to be picked up in a metabolic cage study. We therefore selected an early stage Dox-HFD paradigm and measured energy expenditure within two weeks of gene induction on the HFD. This is at a point when no significant body-weight differences were apparent. Within the sensitivity of our measurements, we observed no marked differences in whole-body energy expenditure (Supplementary Figure 1). More specifically, no significant differences were observed in oxygen-consumption, carbon-dioxide production or respiratory exchange rate (RER) between WT and E4orf1-Tg mice (Supplementary Figure 1). However, and somewhat surprisingly, transgenic mice did appear to exhibit markedly lower total X-beam movements (XT), X-ambulatory (XA) movements and X-fine movements (XF), reflecting grooming behavior (Supplementary Figure 1); this lack in movement and grooming, in addition to the increase in total water consumption for the duration of the experiment. In particular, while glucose tolerance appears comparable between genotypes (Figure 2B), transgenic mice do not utilize/require the same amount of insulin (Figure 2B) due to the induction of E4orf1 in WAT. Combined with the unhealthy WAT evident in the transgenic mice, this implicates an overall metabolically unfavorable phenotype. However, even though trends were apparent in many of the parameters measured in the metabolic cages (such as enhanced food-intake, reduced overall body-weight gain), these measurements failed to give us statistically meaningful data that could explain the lighter body weight on the basis of altered expenditure.

Histological analyses of sWAT and gWAT tissues revealed comparable adipocyte size between WT and E4orf1-Tg H&E stained tissues (Figure 2E). Importantly, perilipin immunohistochemical (IHC) staining demonstrated comparable perilipin-positive staining between WT and E4orf1-Tg sWAT (Figure 2E), indicating that adipocytes in E4orf1-Tg sWAT are viable and the induction of E4orf1 protein is therefore not toxic. Given the low systemic adiponectin levels in E4orf1-Tg mice, we hypothesized that the WAT depots in E4orf1-Tg mice may be dysfunctional. Indeed, Mac2 IHC staining and trichrome staining revealed enhanced macrophage infiltration and fibrosis, evident in E4orf1-Tg sWAT, when compared to WT sWAT (Figure 2E). Such enhanced inflammatory and fibrotic processes indicate that E4orf1-Tg mice undergo unhealthy expansion leading to dysfunctional WAT during metabolic challenge, which further provides some explanation of their impairment in lipid clearance capacity, as observed in Figure 2C. Consistent with a reduction in body-weight gain during Dox-HFD feeding, E4orf1-Tg mice harbor significantly smaller sWAT and gWAT fat-pads than their WT counterparts (Figure 2F). Given the overall unhealthy, inflamed and fibrotic nature of the E4orf1-Tg sWAT fat-pad (Figure 2E), appropriate diet-induced sWAT expansion may be severely impaired. This is evident from the insufficient remodeling of extracellular matrix (ECM) and angiogenic programs that hinder healthy sWAT expansion. Indeed, by utilizing RNA deep-sequencing (RNA-Seq) methodology on sWAT derived from mice that were metabolically challenged with Dox-HFD for two weeks, we identify that gene expression levels of a key angiogenic marker vascular endothelial growth factor A (*Vegf-A*) are significantly down-regulated in E4orf1-Tg sWAT (Supplementary Table 1). Furthermore, several components of fibrosis, ECM remodeling and hypoxia signaling pathways are significantly up-regulated in E4orf1-Tg sWAT. In particular, transforming growth factor β-receptor 1 [*Tgf-βr1*], connective tissue growth factor [*Ctgf*], hypoxia-inducible factor 1-α (*Hif1a*) and several collagens (*Col4a3bp*, *Col12a1*, *Col14a1*) are dysregulated (Supplementary Table 1), collectively substantiating the unhealthy nature of E4orf1 sWAT. Finally, given the inability of E4orf1-Tg mice to appropriately expand their sWAT fat-pad to accommodate surplus dietary lipids, we assessed whether any hepatic steatosis was evident in these mice. Unexpectedly, H&E staining revealed markedly less lipid accumulation in E4orf1-Tg liver tissues (Figure 2E); this was corroborated quantitatively as E4orf1-Tg mice were shown to have an overall reduction in liver tissue weight when normalized to body-weight (Figure 2F), in addition to exhibiting significantly lower hepatic TG levels in comparison to WT mice (Figure 2G).

3.3. Adipose tissue-specific induction of E4orf1 promotes *insulin-independent* up-regulation in p-Akt expression levels

To assess AT insulin signaling in the presence of E4orf1, mice underwent two weeks of Dox-chow feeding (600 mg/kg) and insulin-stimulated phospho-Akt (p-Akt) levels were examined. Interestingly, we observed a significant increase in baseline, non-insulin-stimulated p-Akt expression in E4orf1-Tg sWAT compared to WT sWAT (Figure 3A), while total-Akt expression levels remained unchanged (Supplementary Figure 2). A similar pattern was also observed in E4orf1-Tg BAT, the fat-depot that achieves the highest level of E4orf1 protein induction. Such an increase in p-Akt by E4orf1 under baseline conditions suggests that E4orf1 may activate the insulin-signaling cascade to enhance p-Akt *independently* of insulin. Upon insulin-stimulation (5, 10 and 15 min post insulin injection), conversely, markedly reduced levels of p-Akt expression are evident in E4orf1-Tg sWAT (Figure 3A). While E4orf1 impairs insulin-mediated effects, it raises the question how E4orf1 has the ability to trigger the insulin-signaling cascade in the *absence of insulin*; this is extremely important, particularly in the context of diabetic conditions with conventional insulin resistance. Quantitatively, in the basal un-stimulated state, we further substantiated the significant increase in p-Akt expression in E4orf1-Tg sWAT, by normalizing to total-Akt levels (Figure 3B). A marked reduction in p-Akt expression was further apparent in E4orf1-Tg livers (Figure 3B), suggesting some degree of hepatic insulin resistance as a secondary consequence of the dysfunctional WAT in E4orf1-Tg mice. Upon examination of other targets of the insulin-signaling pathway, we observed a marked reduction in insulin-stimulated p-tyrosine (p-Tyr) (insulin receptor β-subunit and IRS-1) expression levels in E4orf1-Tg sWAT and liver tissues (Figure 3C). Similarly upon Dox-chow feeding, assessing p-ERK, a downstream target of the Ras-mediated pathway, we noticed it to be markedly lower in insulin-stimulated E4orf1-Tg sWAT and liver tissues (Figure 3D). Lower baseline and insulin-stimulated levels of caveolin-1 (Cav-1) p-Tyr 14 were also apparent in sWAT and liver tissues from

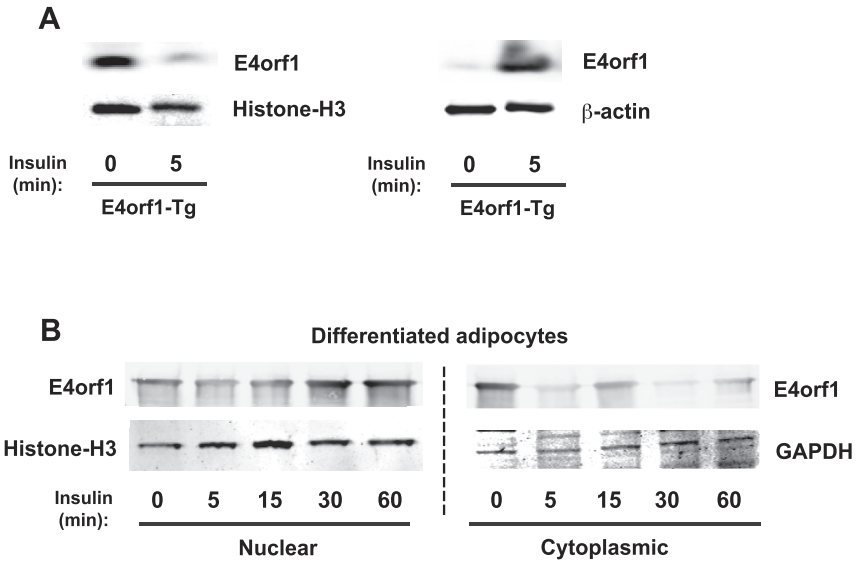

Figure 4: Insulin stimulates the intracellular translocation of the E4orf1 protein from cytosolic to nuclear compartments. (A) Representative Western blots of E4orf1 protein expression in the nuclear fraction, accompanied with the nuclear loading control Histone-H3 (left panel); in addition to cytoplasmic E4orf1 expression with a β-actin control (right panel), from sWAT derived from E4orf1-Tg mice that were injected with insulin (0 min and 5 min post insulin injection [1 U/kg body-weight insulin i.p]). Mice were fed Dox-HFD (600 mg/kg) for three-weeks prior to being fasted overnight (14–16 h). (B) Representative Western blots of E4orf1 protein (top panels) and the nuclear loading control Histone-H3 (bottom left) and the cytoplasmic loading control GAPDH (bottom right) in mature adipocytes that were differentiated from the stromal vascular fraction isolated from E4orf-1Tg BAT. Cells were differentiated for seven-days, then induced with Dox (10 μg/ml) for two-days. Adipocytes were either untreated (0 min) or treated with insulin (5, 15, 30 and 60 min post insulin treatment). Blots showing nuclear fractions are on the left, with cytoplasmic fraction blots on the right.

E4orf1-Tg mice (Figure 3E). Finally, we examined glucose transporter levels in sWAT by immunofluorescence staining, which revealed more prominent Glut4 staining in E4orf1-Tg sWAT, when compared with WT sWAT (Figure 3F).

To examine whether E4orf1 induction alters transcriptional events in sWAT, we performed RNA deep sequencing (RNA-Seq) on sWAT derived from WT and E4orf1-Tg mice following two weeks of Dox-HFD feeding. Transcriptional analyses of key components of the insulin-signaling pathway revealed a significant down-regulation in the insulin receptor, IRS-1/2, PI3K (p85 and p110 subunits) and Glut4 gene expression levels in E4orf1-Tg sWAT compared to WT sWAT (Figure 3G). In contrast, analyses further revealed that numerous genes involved in the Ras-ERK-MAPK-mediated signaling cascade are significantly up-regulated in E4orf1-Tg sWAT, when compared with WT sWAT (Supplementary Table 2). Key genes markedly up-regulated in the Ras-ERK-MAPK pathway in E4orf-1Tg sWAT included *K-Ras* and several activators and substrates of Ras (*Sos1/2*, Ras-*a1*, *R-Ras2*, *Rac1*, *Rap-1a/1b*), in addition to ERK and MAPK genes (*Map2k6*, *Mapk4k3*, *Mapk6* [*Erk3*], *Mapk8* [*Jnk1*]) (Supplementary Table 2). Further RNA-Seq analyses identified that the top most significantly up-regulated genes in E4orf1-Tg sWAT are elongation factor 1-α 2 (*Eef1a2*), protein phosphatase 1 regulatory subunit 3A (*Ppp1r3a*), lipocalin-2 (*Lcn2*) and the protein MAL2 (*Mal2*). Subsequent qPCR analyses confirmed the marked up-regulation of these genes in E4orf1-Tg sWAT, with *Eef1a2* in particular, significantly up-regulated more than 100-fold in transgenic sWAT (Figure 3H). In contrast, the most significantly down-regulated genes in E4orf1-Tg sWAT included cytochrome P450 2E1 (*Cyp2e1*), probable leucyl-tRNA synthetase (*Lars2*), complement factor D (adipsin) (*Cfd*), solute carrier family 1 member 5 (neutral amino acid transporter) (*Slc1a5*), carboxylesterase 1D (*Ces1d*) and alanine-glyoxylate aminotransferase 2 (*Agt2*); qPCR further confirmed the significant down-regulation of these genes in E4orf1-Tg sWAT (Figure 3I).

3.4. Insulin stimulates the intracellular re-localization of E4orf1 protein from cytosolic to nuclear compartments

Our initial observations revealed that insulin enhances E4orf1 protein expression in the nuclear fraction of sWAT following 5 min post insulin injection (Figure 4A), suggesting a potential insulin-stimulated cytoplasmic re-localization of the E4orf1 protein. To explore this phenomenon further, we isolated the stromal vascular fraction from BAT derived from E4orf1-Tg mice post Dox-chow feeding and differentiated the cells into mature adipocytes. We then stimulated adipocytes with insulin and assessed any potential intracellular movement of the E4orf1 protein. Figure 4B shows a time-dependent effect of insulin to stimulate a re-localization of the E4orf1 protein, a translocation from cytoplasmic compartments to the nuclear fractions. Consistent with our observations, recent studies in a cancer setting, reported that the E4orf1 protein translocates from cytoplasmic to nucleus compartments to activate Myc [19].

3.5. E4orf1 induction impairs BAT and promotes whitening

The highest degree of E4orf1 induction is achieved in the BAT depot (Figure 1A). As such, we wanted to assess whether E4orf1 induction alters the transcriptional browning signature program in BAT. Interestingly, following two weeks of Dox-HFD feeding, gene markers of browning (*Ucp1*, *Pgc1α*, *Cidea*, *Otop1* and *Prdm16*) were significantly down-regulated in E4orf1-Tg BAT compared to WT BAT (Figure 5A). Visually, the BAT depot in E4orf1-Tg mice appeared to have whitened in color, such that very little true BAT was evident. By utilizing Illumina microarrays, we identified significantly altered gene clusters in BAT derived from E4orf1-Tg mice that underwent two weeks of Dox-HFD feeding. Supplementary Table 3 highlights a significant suppression in the angiogenic marker *Vegf-B* in E4orf1-Tg BAT. Conversely, a significant up-regulation in several markers of fibrosis and ECM remodeling genes (*Tgfbi*, *Tgf-βr1*, *Smad3/4* and many matrix metallopeptidases [MMPs]) was apparent in E4orf1-Tg BAT (Supplementary

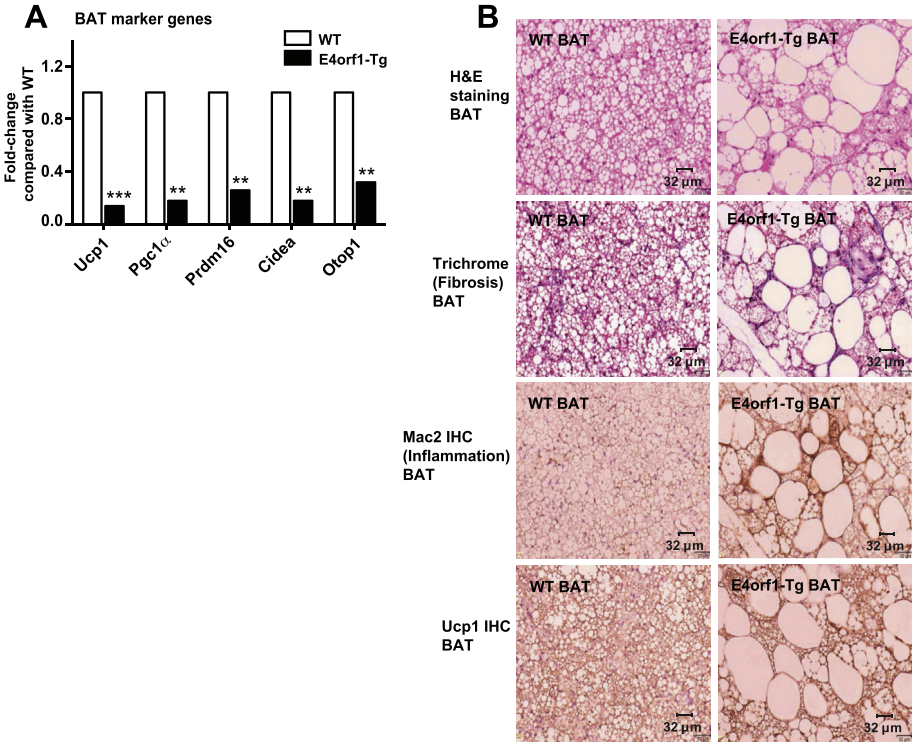

Figure 5: E4orf1 induction promotes whitening of BAT. (A) Real-time qPCR data showing BAT marker gene expression levels (*Ucp1*, *Pgc1α*, *Prdm16*, *Cidea* and *Otop1*) in BAT derived from WT mice *versus* E4orf1-Tg mice following three-weeks of Dox-HFD (600 mg/kg) feeding. (Student's *t*-test, $^{**}P < 0.01$; $^{***}P < 0.001$). (B) Representative images of BAT derived from WT mice *versus* E4orf1-Tg mice that underwent H&E staining (top panel), Trichrome staining (second panel), Mac2 IHC (third panel) and Ucp1 IHC (fourth panel). Scale bar: 32 μm.

Table 3). Similar to sWAT, numerous collagens were also markedly up-regulated in E4orf1-Tg BAT (Supplementary Table 3), suggesting unhealthy fibrotic AT. In line with the gene expression data, histological examination through H&E staining revealed markedly disorganized and enlarged lipid-laden adipocytes in E4orf1-Tg BAT (Figure 5B). Further, consistent with the gene expression data (Supplementary Table 3), trichrome staining revealed enhanced tissue fibrosis in E4orf1-Tg BAT (Figure 5B). E4orf1-Tg BAT also displayed enhanced Mac2-positive staining (Figure 5B), indicating inflamed and unhealthy AT, similar to that observed for E4orf1-Tg sWAT (Figure 2E). However, despite the gene expression data highlighting a marked reduction in the browning signature program in E4orf1-Tg BAT (Figure 5A), Ucp1 IHC showed no striking differences in Ucp1-positive staining between WT BAT and E4orf1-Tg BAT (Figure 5B). This suggests that even though mRNA levels are reduced, UCP1 protein levels are maintained, either through enhance translational efficacy or a prolonged half-life for UCP1 protein.

4. DISCUSSION

By taking advantage of the properties of E4orf1, we generated and validated an inducible mouse model that allows us to alter the classical signaling events in the distal branches of the insulin signal transduction pathway in adipose tissue, in an insulin-independent manner. The phenotypic outcome *in vivo* of such a perturbation results in the adipose tissue-specific E4orf1 transgenic mouse (the E4orf1-Tg mouse) exhibiting lower body-weight gain under metabolically challenging conditions and 'insulin-sparing' characteristics during glucose tolerance tests. Transgenic mice also exhibit reduced circulating adiponectin levels, inflamed and fibrotic WAT; however, the mice are protected from diet-induced hepatic steatosis. This model, therefore, defies many expectations regarding adiposity, healthy state of adipose tissue, adiponectin levels and insulin sensitivity. *Ex vivo* analyses revealed that E4orf1 promotes up-regulation of p-Akt expression in adipose tissues in the absence of insulin. Furthermore, microarray analyses pinpointed that specifically under metabolic challenge, enhanced Ras-ERK-MAPK signaling in E4orf1-Tg sWAT could serve as a potential alternative route to bypass classical insulin signaling events. Interestingly, insulin negatively regulates E4orf1 protein expression in sWAT and, moreover, stimulates the intracellular re-localization of E4orf1 protein from cytosolic to nuclear compartments. Finally under metabolic challenge, E4orf1-Tg mice exhibit whitening of BAT, as a reduction in transcriptional profile of classical browning markers, in addition to enlarged lipid-laden hypertrophic adipocytes was evident. Nevertheless, glucose tolerance remained normal in these mice. Taken together, Figure 6 highlights the *in vivo* action of E4orf1 in adipocytes.

Previous *in vitro* studies utilizing 3T3-L1 adipocytes described that E4orf1 increases Glut4 translocation to the plasma membrane and glucose uptake in an insulin-independent fashion, as insulin signaling was preserved despite the presence of an insulin receptor knockdown [20–22]. This suggests that E4orf1-mediated signaling harbors 'insulin-sparing' characteristics. Consistent with this, while glucose tolerance was comparable to wild-type mice, E4orf1-Tg mice lacked the transient insulin spike typically observed in response to a glucose bolus. This could indicate that E4orf1-Tg mice do not require the same amount of insulin to clear exogenous glucose, rather maintain adequate activation of the insulin signaling cascade through E4orf1-mediated signaling. Indeed, in the fasting state with low levels of insulin, we observed an E4orf1-induced up-regulation in p-Akt expression in adipose tissues, further highlighting the insulin-independent

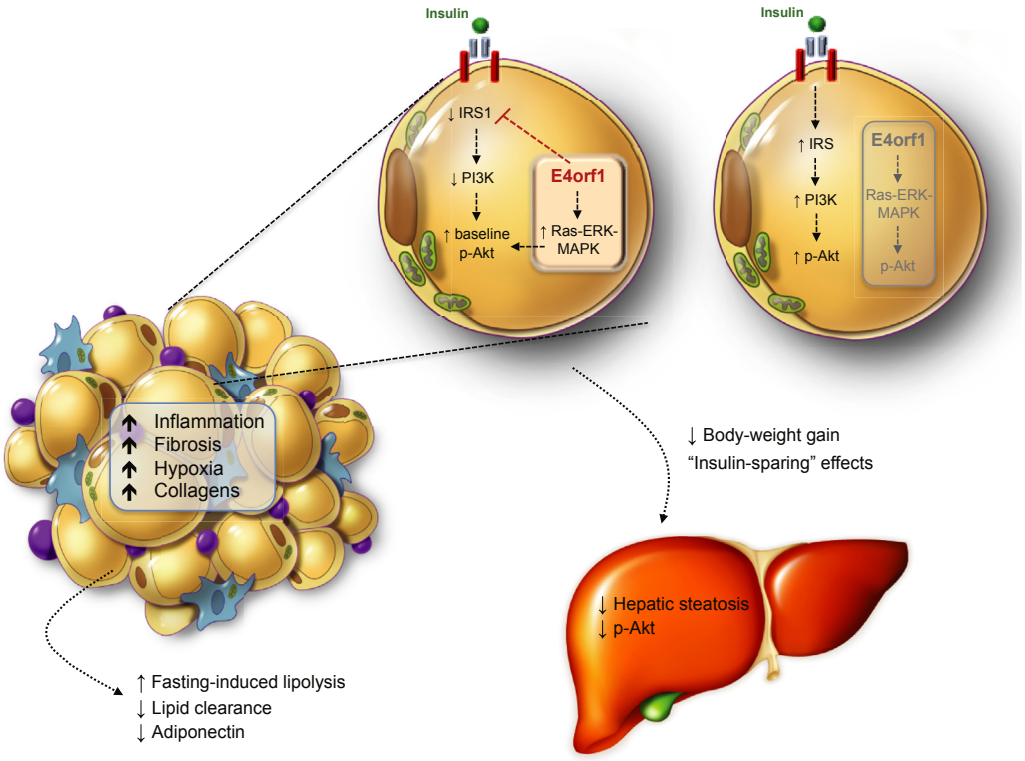

Figure 6: *In vivo* mechanistic action of E4orf1 in the white adipocyte. E4orf1 induction in WAT promotes inflammation, fibrosis, hypoxia and an increase in expression of several collagens. At the level of the white adipocyte, in the presence of excess insulin, the classical insulin signaling transduction pathway is activated to enhance p-Akt. In the absence of insulin, an induction in E4orf1 within the adipocyte can preserve activation of the insulin signaling pathway by triggering a Ras-ERK-MAPK branch of signaling that ultimately enhances p-Akt expression. Consequently at the whole-body level, E4orf1-Tg mice exhibit reduced body-weight gain under metabolic challenge, an increase in fasting-induced lipolysis, reduced adiponectin levels, protection from HFD-induced hepatic steatosis, in addition to key "insulin-sparing" effects during glucose tolerance testing.

signaling properties of E4orf1. In parallel, we recently utilized the adiponectin promoter-driven rtTA cassette coupled with a TRE-CRE transgenic mouse to inducibly eliminate from the mature adipocyte the floxed protein *phosphatase and tensin homolog* (PTEN) locus, a protein that inhibits cellular insulin signaling transduction (*Morley, Xia and Scherer; Nat. Comm., in press*). It is interesting to note that in the case of PTEN elimination in the adipocyte, the loss of PTEN in the mature adipocyte leads to increased insulin sensitivity in multiple peripheral tissues, and a greatly improved metabolic phenotype upon acute and chronic exposure to high fat diets. These observations highlight the major differences arising from subtle manipulations of the pathway with one and the same cell. The adipocyte-specific PTEN knock out has elevated not only baseline levels of p-Akt but also, in contrast to the model presented here, much higher and longer lasting amplitudes of p-Akt signaling post exposure to insulin. This triggers differential responses in the liver, and results in a completely differential systemic read out with respect to metabolic homeostasis.

Previous studies have described E4orf1 as an obesogenic agent that induces adiposity by increasing glucose uptake and promoting chronic inflammation in adipose tissues [32–34]. Here, however, E4orf1-Tg mice exhibit a marked reduction in body-weight gain during Dox-HFD feeding. Such a discrepancy between cultured systems and an *in vivo* environment suggests that E4orf1 may promote adiposity in an isolated system. However, the *in vivo* induction of E4orf1 specifically in adipose tissues may involve additional components that influence the adiposity-inducing properties of E4orf1. Consistent with *in vitro* studies, we find that E4orf1 increases monocyte chemoattractant protein-1 (MCP-1) levels in fat-pads, to create a chronic pro-inflammatory state [32,35]. Our data also reveal that E4orf1-Tg mice harbor inflamed and fibrotic adipose tissues, indicating 'unhealthy' WAT expansion during the onset of diet-induced obesity. The latter is further reflected by the fact that E4orf1-Tg mice harbor markedly lower circulating levels of adiponectin, a typical hallmark of metabolically unhealthy WAT [30,36,37]. Interestingly, transgenic mice are protected from Dox-HFD-induced hepatic steatosis, despite exhibiting markedly lower fat-pads weights. This is in agreement with previous reports demonstrating that E4orf1 improves hyperglycemia and hepatic steatosis in HFD-fed mice, in addition to lowering hepatic lipid levels in seropositive subjects [38]. Given that we observe no marked differences in food-intake between genotypes, this would suggest an increase in whole-body energy expenditure.

Numerous actions of insulin are mediated through the PI3-kinase/Akt pathway. More specifically, Akt plays a central role in mediating several of insulin's actions on metabolism by regulating the expression and activity of a wide range of intracellular substrates that play key roles in a range of biological processes [39–41]. Here, we see that p-Akt expression is enhanced in E4orf1-Tg sWAT under basal conditions. However, it is reduced under insulin-stimulated conditions. Consistent with these observations, E4orf1 enhances translocation of Glut4 and thus increases glucose uptake in adipocytes through activation of the Akt and Ras signaling pathways [38,42]. Of note, insulin is required for WAT to development normally, minimally to allow a build up of lipids through suppression of lipolysis, a scenario most dramatically visualized in a type 1 diabetic setting. This is in contrast to the chronic baseline stimulation of Akt by E4orf1 described here, which actually has a negative impact on WAT development and function.

A second essential branch of the insulin signaling pathway is the Ras-Raf-Sos-MEK-ERK pathway [43]. Son-of-sevenless (Sos) is a guanine nucleotide exchange factor that activates the GTP-bound form of Ras (Ras-GTP). Ras-GTP then stimulates downstream effectors, such as the Ser/Thr kinase Raf, which, in turn, activate MEK1 and 2 to phosphorylate MAP kinases extracellular-signal-regulated kinase 1 (ERK1) and 2 [43]. Here, RNA-Seq gene-clustering analyses identified numerous genes in the Ras-ERK-MAPK signaling pathway that are up-regulated in E4orf1-Tg sWAT under metabolic challenge. Key genes included *K-Ras* and several activators and substrates of Ras (*Sos1/2*, *Ras-a1*, *R-Ras2*, *Rac1*, *Rap-1a/1b*), in addition to several ERK and MAPK genes (*Map2k6*, *Mapk4k3*, *Mapk6* [*Erk3*], *Mapk8* [*Jnk1*]). Given that stress kinases, such as ERK and c-Jun N-terminal kinase (JNK) inhibit insulin signaling by inducing inhibitory serine/threonine phosphorylation of the insulin receptor and IRS proteins [43,44], the up-regulation of ERK and JNK in transgenic sWAT suggests a potential inhibition of the proximal insulin signaling pathway at IRS, with activation of an alternative distal insulin signaling route via Ras-mediated signaling. Indeed, in the absence of insulin and insulin receptor signaling, E4orf1 inhibits IRS1/2 phosphorylation and enhances Ras activity to activate PKB/Akt in cultured 3T3-L1 adipocytes. This ultimately promotes cellular glucose uptake [21–23]. As such, E4orf1 has been suggested to enhance cellular glucose uptake by bypassing proximal insulin signaling. Of note, multiple signaling pathways can activate Akt and ERK cascades [45]. In particular, serine phosphorylation of IRS proteins can inhibit recruitment to PI3K, thus minimizing its activation [46], and can result in degradation of IRS-1 [47] and subsequent inhibition of distal insulin signaling. Our future studies will have to address whether serine phosphorylation of IRS proteins is a potential target for E4orf1 mediated effects in adipocytes.

In summary, we generate and characterize a novel mouse model of E4orf1 induction specifically in adipose tissue, which harbors 'insulin-sparing' characteristics. This phenomenon arises from activation of a Ras-ERK-MAPK signaling pathway that enhances insulin-independent p-Akt expression.

ACKNOWLEDGMENTS

We kindly thank J. Song and S. Connell for technical assistance, in addition to the rest of the Scherer laboratory for helpful discussions. We would also like to thank R. Hammer and the UTSW Transgenic Core Facility for the generation of mouse models, as well as the UTSW Metabolic Core Facility. The authors were supported by US National Institutes of Health grants R01-DK55758, R01-DK099110 and P01DK088761 (to P.E.S.). C.M.K. was supported by a fellowship from the Juvenile Diabetes Foundation (JDRF 3-2008-130). Z.V.W. is supported by a Scientist Development Grant from the American Heart Association (14SDG18440002). A grant from Vital Health Interventions (NVD) also in part contributed to the study. P.E.B. was supported by the Jean D. Wilson Center for Biomedical Research.

AUTHOR CONTRIBUTIONS

C.M.K. conducted all experiments and wrote the manuscript, except the portions indicated below. V.G.M. performed the SVF isolations from BAT, in addition to the corresponding adipocyte differentiation and Western blotting for E4orf1 protein. Z.V.W. generated the TRE-E4orf1-Tg mice. P.E.B. assisted with protocols and interpretation for the SVF and adipocyte differentiation experiments, in addition to data interpretation. N.V.D. contributed E4orf1 antibodies and cDNAs, in addition to helping with experimental design and data interpretation. P.E.S. was involved in experimental design, experiments, data analysis, and interpretation, in addition to writing of the manuscript.

DISCLOSURE STATEMENT

NVD has applied for or holds the following patents. United States # 6,127,113—Viral obesity methods and compositions; #6,664,050—Viral obesity methods and compositions; #8,008,436B2: Adenovirus 36 E4orf1 gene & protein & their uses; Europe #11741354.2—Adenovirus Ad36 E4orf1 protein for prevention and treatment of non-alcoholic fatty liver disease; New Zealand #606236—Adenovirus Ad36 E4orf1 protein for prevention and treatment of non-alcoholic fatty liver disease; as well as additional patents currently filed.

APPENDIX A. SUPPLEMENTARY DATA

Supplementary data related to this article can be found at http://dx.doi.org/10.1016/j.molmet.2015.07.004.

REFERENCES

[1] Samuel, V.T., Petersen, K.F., Shulman, G.I., 2010. Lipid-induced insulin resistance: unravelling the mechanism. Lancet 375(9733):2267—2277.

[2] Taniguchi, C.M., Emanuelli, B., Kahn, C.R., 2006. Critical nodes in signalling pathways: insights into insulin action. Nature Reviews Molecular Cell Biology 7(2):85—96.

[3] Abel, E.D., Peroni, O., Kim, J.K., Kim, Y.B., Boss, O., Hadro, E., et al., 2001. Adipose-selective targeting of the GLUT4 gene impairs insulin action in muscle and liver. Nature 409(6821):729—733.

[4] Lo, K.A., Labadorf, A., Kennedy, N.J., Han, M.S., Yap, Y.S., Matthews, B., et al., 2013. Analysis of in vitro insulin-resistance models and their physiological relevance to in vivo diet-induced adipose insulin resistance. Cell Reports 5(1):259—270.

[5] Adams-Huet, B., Devaraj, S., Siegel, D., Jialal, I., 2014. Increased adipose tissue insulin resistance in metabolic syndrome: relationship to circulating adipokines. Metabolic Syndrome and Related Disorders 12(10):503—507.

[6] Bae, S.S., Cho, H., Mu, J., Birnbaum, M.J., 2003. Isoform-specific regulation of insulin-dependent glucose uptake by Akt/protein kinase B. Journal of Biological Chemistry 278(49):49530—49536.

[7] Bluher, M., Michael, M.D., Peroni, O.D., Ueki, K., Carter, N., Kahn, B.B., et al., 2002. Adipose tissue selective insulin receptor knockout protects against obesity and obesity-related glucose intolerance. Developmental Cell 3(1):25—38.

[8] Ussar, S., Bezy, O., Bluher, M., Kahn, C.R., 2012. Glypican-4 enhances insulin signaling via interaction with the insulin receptor and serves as a novel adipokine. Diabetes 61(9):2289—2298.

[9] Rice, K.M., Turnbow, M.A., Garner, C.W., 1993. Insulin stimulates the degradation of IRS-1 in 3T3-L1 adipocytes. Biochemical and Biophysical Research Communications 190(3):961—967.

[10] Zierath, J.R., Houseknecht, K.L., Gnudi, L., Kahn, B.B., 1997. High-fat feeding impairs insulin-stimulated GLUT4 recruitment via an early insulin-signaling defect. Diabetes 46(2):215—223.

[11] Gao, Z., Zuberi, A., Quon, M.J., Dong, Z., Ye, J., 2003. Aspirin inhibits serine phosphorylation of insulin receptor substrate 1 in tumor necrosis factor-treated cells through targeting multiple serine kinases. Journal of Biological Chemistry 278(27):24944—24950.

[12] Clark, S.F., Molero, J.C., James, D.E., 2000. Release of insulin receptor substrate proteins from an intracellular complex coincides with the development of insulin resistance. Journal of Biological Chemistry 275(6):3819—3826.

[13] Tan, S.X., Ng, Y., Burchfield, J.G., Ramm, G., Lambright, D.G., Stockli, J., et al., 2012. The Rab GTPase-activating protein TBC1D4/AS160 contains an atypical phosphotyrosine-binding domain that interacts with plasma membrane phospholipids to facilitate GLUT4 trafficking in adipocytes. Molecular and Cellular Biology 32(24):4946—4959.

[14] Teruel, T., Hernandez, R., Lorenzo, M., 2001. Ceramide mediates insulin resistance by tumor necrosis factor-alpha in brown adipocytes by maintaining Akt in an inactive dephosphorylated state. Diabetes 50(11):2563–2571.
[15] Yamauchi, T., Kamon, J., Waki, H., Terauchi, Y., Kubota, N., Hara, K., et al., 2001. The fat-derived hormone adiponectin reverses insulin resistance associated with both lipoatrophy and obesity. Nature Medicine 7(8):941–946.
[16] Berg, A.H., Combs, T.P., Du, X., Brownlee, M., Scherer, P.E., 2001. The adipocyte-secreted protein Acrp30 enhances hepatic insulin action. Nature Medicine 7(8):947–953.
[17] Semple, R.K., Soos, M.A., Luan, J., Mitchell, C.S., Wilson, J.C., Gurnell, M., et al., 2006. Elevated plasma adiponectin in humans with genetically defective insulin receptors. Journal of Clinical Endocrinology and Metabolism 91(8): 3219–3223.
[18] Semple, R.K., Halberg, N.H., Burling, K., Soos, M.A., Schraw, T., Luan, J., et al., 2007. Paradoxical elevation of high-molecular weight adiponectin in acquired extreme insulin resistance due to insulin receptor antibodies. Diabetes 56(6):1712–1717.
[19] Thai, M., Graham, N.A., Braas, D., Nehil, M., Komisopoulou, E., Kurdistani, S.K., et al., 2014. Adenovirus E4ORF1-induced MYC activation promotes host cell anabolic glucose metabolism and virus replication. Cell Metabolism 19(4):694–701.
[20] Krishnapuram, R., Dhurandhar, E.J., Dubuisson, O., Hegde, V., Dhurandhar, N.V., 2013. Doxycycline-regulated 3T3-L1 preadipocyte cell line with inducible, stable expression of adenoviral E4orf1 gene: a cell model to study insulin-independent glucose disposal. PLoS One 8(3):e60651.
[21] Krishnapuram, R., Kirk-Ballard, H., Dhurandhar, E.J., Dubuisson, O., Messier, V., Rabasa-Lhoret, R., et al., 2013. Insulin receptor-independent upregulation of cellular glucose uptake. International Journal of Obesity (London) 37(1):146–153.
[22] Wang, Z.Q., Cefalu, W.T., Zhang, X.H., Yu, Y., Qin, J., Son, L., et al., 2008. Human adenovirus type 36 enhances glucose uptake in diabetic and nondiabetic human skeletal muscle cells independent of insulin signaling. Diabetes 57(7):1805–1813.
[23] Dhurandhar, E.J., Dubuisson, O., Mashtalir, N., Krishnapuram, R., Hegde, V., Dhurandhar, N.V., 2011. E4orf1: a novel ligand that improves glucose disposal in cell culture. PLoS One 6(8):e23394.
[24] Wang, Q.A., Tao, C., Gupta, R.K., Scherer, P.E., 2013. Tracking adipogenesis during white adipose tissue development, expansion and regeneration. Nature Medicine 19(10):1338–1344.
[25] Livak, K.J., Schmittgen, T.D., 2001. Analysis of relative gene expression data using real-time quantitative PCR and the 2(-Delta Delta C(T)) Method. Methods 25(4):402–408.
[26] Folch, J., Lees, M., Sloane Stanley, G.H., 1957. A simple method for the isolation and purification of total lipides from animal tissues. Journal of Biological Chemistry 226(1):497–509.
[27] Gupta, R.K., Arany, Z., Seale, P., Mepani, R.J., Ye, L., Conroe, H.M., et al., 2010. Transcriptional control of preadipocyte determination by Zfp423. Nature 464(7288):619–623.
[28] Dubuisson, O., Dhurandhar, E.J., Krishnapuram, R., Kirk-Ballard, H., Gupta, A.K., Hegde, V., et al., 2011. PPARgamma-independent increase in glucose uptake and adiponectin abundance in fat cells. Endocrinology 152(10):3648–3660.
[29] Schraw, T., Wang, Z.V., Halberg, N., Hawkins, M., Scherer, P.E., 2008. Plasma adiponectin complexes have distinct biochemical characteristics. Endocrinology 149(5):2270–2282.
[30] Ye, R., Scherer, P.E., 2013. Adiponectin, driver or passenger on the road to insulin sensitivity? Molecular Metabolism 2(3):133–141.
[31] Shetty, S., Kusminski, C.M., Scherer, P.E., 2009. Adiponectin in health and disease: evaluation of adiponectin-targeted drug development strategies. Trends in Pharmacological Sciences 30(5):234–239.
[32] Na, H.N., Hong, Y.M., Ye, M.B., Park, S., Kim, I.B., Nam, J.H., 2014. Adenovirus 36 attenuates weight loss from exercise but improves glycemic control by increasing mitochondrial activity in the liver. PLoS One 9(12): e114534.
[33] Dubuisson, O., Day, R.S., Dhurandhar, N.V., 2015. Accurate identification of neutralizing antibodies to adenovirus Ad36, -a putative contributor of obesity in humans. Journal of Diabetes and its Complications 29(1):83–87.
[34] Almgren, M., Atkinson, R., He, J., Hilding, A., Hagman, E., Wolk, A., et al., 2012. Adenovirus-36 is associated with obesity in children and adults in Sweden as determined by rapid ELISA. PLoS One 7(7):e41652.
[35] Na, H.N., Nam, J.H., 2012. Adenovirus 36 as an obesity agent maintains the obesity state by increasing MCP-1 and inducing inflammation. Journal of Infectious Diseases 205(6):914–922.
[36] Turer, A.T., Scherer, P.E., 2012. Adiponectin: mechanistic insights and clinical implications. Diabetologia 55(9):2319–2326.
[37] Sun, K., Kusminski, C.M., Scherer, P.E., 2011. Adipose tissue remodeling and obesity. Journal of Clinical Investigation 121(6):2094–2101.
[38] Krishnapuram, R., Dhurandhar, E.J., Dubuisson, O., Kirk-Ballard, H., Bajpeyi, S., Butte, N., et al., 2011. Template to improve glycemic control without reducing adiposity or dietary fat. American Journal of Physiology–Endocrinology and Metabolism 300(5):E779–E789.
[39] Manning, B.D., Cantley, L.C., 2007. AKT/PKB signaling: navigating downstream. Cell 129(7):1261–1274.
[40] Whiteman, E.L., Cho, H., Birnbaum, M.J., 2002. Role of Akt/protein kinase B in metabolism. Trends in Endocrinology & Metabolism 13(10):444–451.
[41] Alessi, D.R., Downes, C.P., 1998. The role of PI 3-kinase in insulin action. Biochimica et Biophysica Acta 1436(1–2):151–164.
[42] Vangipuram, S.D., Yu, M., Tian, J., Stanhope, K.L., Pasarica, M., Havel, P.J., et al., 2007. Adipogenic human adenovirus-36 reduces leptin expression and secretion and increases glucose uptake by fat cells. International Journal of Obesity (London) 31(1):87–96.
[43] Boucher, J., Kleinridders, A., Kahn, C.R., 2014. Insulin receptor signaling in normal and insulin-resistant states. Cold Spring Harbor Perspectives in Biology 6(1).
[44] Aguirre, V., Uchida, T., Yenush, L., Davis, R., White, M.F., 2000. The c-Jun NH(2)-terminal kinase promotes insulin resistance during association with insulin receptor substrate-1 and phosphorylation of Ser(307). Journal of Biological Chemistry 275(12):9047–9054.
[45] Draznin, B., 2006. Molecular mechanisms of insulin resistance: serine phosphorylation of insulin receptor substrate-1 and increased expression of p85alpha: the two sides of a coin. Diabetes 55(8):2392–2397.
[46] Aguirre, V., Werner, E.D., Giraud, J., Lee, Y.H., Shoelson, S.E., White, M.F., 2002. Phosphorylation of Ser307 in insulin receptor substrate-1 blocks interactions with the insulin receptor and inhibits insulin action. J Biol Chem 277(2):1531–1537.
[47] Shah, O.J., Wang, Z., Hunter, T., 2004. Inappropriate activation of the TSC/Rheb/mTOR/S6K cassette induces IRS1/2 depletion, insulin resistance, and cell survival deficiencies. Curr Biol 14(18):1650–1656.

